Research Paper

METTL3 promotes cell cycle progression via m⁶A/YTHDF1-dependent regulation of *CDC25B* translation

Huifeng Li[1, 2*], Ying Zhong[2*], Guangxu Cao[3*], Hezhan Shi[2], Yiyao Liu[1], Lingfeng Li[2], Peidi Yin[2], Jialing Chen[2], Zhendong Xiao[4✉], Bin Du[1✉]

1. Department of Pathology, Shanghai First Maternity and Infant Hospital, Tongji University, Shanghai 200120, China.
2. Department of Pathology, School of Medicine, Jinan University, Guangzhou 510632, China.
3. Department of Gynecology, Shanghai East Hospital, School of Medicine, Tongji University, Shanghai 200120, China.
4. The Third Affiliated Hospital, Sun Yat-Sen University, Guangzhou 510630, China.

*These authors contribute equally.

✉ Corresponding authors: Bin Du: E-mail: doctordu@hotmail.com. Zhendong Xiao: E-mail: xiaozhend@mail.sysu.edu.cn

Abstract

The cell cycle machinery controls cell proliferation and the dysregulation of the cell cycle lies at the heart of carcinogenesis. Thus, exploring the unknown regulators involved in the cell cycle not only contribute to better understanding of cell proliferation but also provide substantial improvement to cancer therapy. In this study, we identified that the expression of methyltransferase METTL3 was upregulated in the M phase. Overexpression of METTL3 facilitated cell cycle progression, induced cell proliferation *in vitro* and enhanced tumorigenicity *in vivo*, while knockdown of METTL3 reversed these processes. METTL3 induced *CDC25B* mRNA m⁶A modification in the M phase, which accelerated the translation of *CDC25B* mRNA through YTHDF1-dependent m⁶A modification. Clinical data analysis showed that METTL3 and CDC25B were highly expressed in cervical cancer. Our work reveals that a new mechanism regulates cell cycle progression through the METTL3/m⁶A/CDC25B pathway, which provides insight into the critical roles of m⁶A methylation in the cell cycle.

Key words: METTL3, cell cycle, m⁶A

Introduction

As a ubiquitous and complex process, the cell cycle is the core event that regulates cell proliferation, and it is closely related to carcinogenesis [1, 2]. The cell cycle includes DNA synthesis (S) and mitosis (M) phases, which are separated by a gap phase; the phases progress in the order G1-S-G2-M. Cell cycle transitions are mainly driven by Cyclins and Cyclin-Dependent Kinases (CDKs) [3]. Moreover, there are a series of checkpoints to ensure that each stage of the cell cycle is completed before the next stage is initiated. Progression through the G1 phase is mainly controlled by Cyclin D1 and CDK4/6, while the CDK2/Cyclin E complex controls progression from the G1 phase to the S phase. The G2/M transition is driven by CDK1/Cyclin B complexes and

many other regulators, such as WEE1(WEE1 G2 checkpoint kinase), PLK1(polo like kinase 1) and cell division cyclin 25 (CDC25) [4]. The CDC25 family includes three homologous isomers (CDC25A, CDC25B and CDC25C) and is involved in cell cycle progression by controlling the phosphorylation state of CDKs. CDC25B, considered a "trigger" phosphatase, is associated with the initial activation of CDK1/cyclin B at the centrosome during the G2/M transition [5, 6]. Additionally, CDC25B is reported to be a potential oncogene that is highly expressed in tumors [7-9]. Previous studies show that cell cycle dysregulation is a central hallmark of oncogenesis and that the activity of cellular proteins implicated in cell cycle regulation is frequently altered in tumor cells,

which protects tumor cells from different types of stress and promotes tumor progression [9, 10]. Thus, cell cycle regulators are expected to be promising targets for cancer therapy. Palbociclib (CDK4/6 inhibitor) and Milciclib (pan-CDK inhibitor) have been approved by the Food and Drug Administration (FDA), representing a promising new area of anticancer drug development [11, 12]. However, series of unknown regulators involves in the cell cycle remaining to be researched.

N6-Methyladenosine (m6A) is the most common internal modification of eukaryotic mRNAs [13]. This reversible and dynamic process is mainly catalyzed by methyltransferase complexes, including methyl-transferase-like 3 (METTL3)/methyltransferase like 14 (METTL14) and Wilms' tumor 1-associating protein (WTAP), which have been designated "writers". m6A modification can be reversed by m6A demethylases (erasers), such as fat mass and obesity-associated protein (FTO) and AlkB homolog 5 (ALKBH5). Factors that recognize and bind to specific modifications have been identified as "readers" and mainly include the YTH m6A RNA binding protein 1-3 (YTHDF1-3), YTH domain-containing 1–2 (YTHDC1-2) and insulin-like growth factor 2 mRNA binding protein 2 (IGF2BP2) [14-18]. Accumulating evidence has shown that m6A modifications can regulate mRNA fate and function by influencing mRNA stability, splicing, transport, localization and translation. Moreover, m6A modifications participate in many diverse biological processes, including tissue development, DNA damage responses, sex determination, and tumorigenesis [19-21].

m6A modification has been implicated in regulating the expression of genes related to the cell cycle. It was reported that FTO regulates cell cycle progression in an m6A-CCNA2-YTHDF2-dependent manner [22]. Downregulation of YTHDF1 expression inhibits non-small-cell lung carcinoma (NSCLC) cell proliferation by regulating the translation of *CDK2*, *CDK4*, and *CCND1* [23]. IGF2BP3, one of the m6A readers, regulates the cell cycle progression and angiogenesis of colon cancer by reading the m6A modifications of *CCND1* and *VEGF*, respectively [24]. These studies suggest that m6A modification potentially plays a role in cell cycle regulation. However, how transcriptomic m6A changes in every phase of the cell cycle, including the G1, S, G2, and M phases, and its function remain unexplored.

In the current study, we found that METTL3 expression was upregulated and was associated with high m6A levels in the M phase of the cell cycle. Functionally, METTL3 facilitated cell cycle progression and induced cell proliferation *in vitro* and *in vivo*. In addition, we identified *CDC25B* as the downstream target of METTL3 and verified that the METTL3-modulated m6A modification of *CDC25B* was recognized by YTHDF1, contributing to the translation of *CDC25B* mRNA in the M phase. Overall, our work is the first to reveal that METTL3 regulates cell cycle progression by controlling the G2/M transition in an METTL3-m6A-CDC25B-dependent manner, which provides insight into the critical roles of m6A methylation in cell cycle regulation.

Results

METTL3 expression was elevated and correlated with the highest m6A level in the M phase

To obtain the transcriptional profiles of the HeLa cell cycle, we performed cell cycle synchronization by using the double-block method with thymidine and nocodazole. The method described in Figure S1A utilizes a double thymidine block (an inhibitor of DNA synthesis) followed by treatment of cells with nocodazole (a mitotic inhibitor) to obtain large cell populations at distinct phases of the cell cycle. The cell cycle synchronization efficiency was confirmed by Western blotting and qPCR analyses of markers including CCNE, CCNA2 and CCNB1, which represent the S, G2 and M phases, respectively. The results shown in Figure S1B and Figure S1C indicated that the cell cycle synchronization model was successfully established, which was consistent with a previous study [25]. According to DESeq analysis (based on the following criteria: fold change > 2 and P < 0.05), we identified differentially expressed genes of each comparison group. As a process when one parent cell physically divides into two daughter cells, the M phase might be the most active phase of the mitosis cell cycle. Comprehensive and systematic investigations of the mechanisms regulating the M phase may provide important clues to gain an extensive understanding of cell cycle regulation. Thus, we analyzed the differentially expressed genes in M phase compared to other cell cycle phases (G1 phase, S phase and G2 phase). Totally, 13 up-regulated genes and 121 down-regulated genes were identified (Figure 1A). Interestingly, METTL3, one of the main methyltransferase, was upregulated in the M phase compared to other phases, which were further confirmed by qPCR and Western blotting assays (Figure 1B). Moreover, we compared the m6A distribution in each phase of the cell cycle and found increased global m6A levels in the M phase (Figure 1D). Furthermore, the mRNA and protein expression levels of the primary m6A methyltransferase and demethylase genes in the G1, S, G2 and M phases were also detected by qPCR and Western blotting

assays. In addition to METTL3, there was no significant difference in the expression of the other main m6A methyltransferase and demethylase genes during cell cycle progression (Figure 1B and 1C). Moreover, the knockdown of METTL3 significantly downregulated the m6A level in cells in the M phase (Figure 1E), which confirmed the methylation activity of METTL3 in the cell cycle. Overall, our results indicated that METTL3 expression is elevated and correlated with the highest m6A level in the M phase. Recently, METTL3 has been reported to regulate the S-phase progression in the cell cycle of fibroblasts through the METTL3-YTHDF2-CCND1 pathway, which ultimately affects fat formation [26]. This result implied that METTL3 and even m6A modification may be associated with different regulatory pathways in various types of cells and different pathological processes.

METTL3 significantly facilitated cell cycle progression and promoted cell growth *in vitro*

To determine the biological function of METTL3,

we established stable METTL3-knockdown and METTL3-overexpression HeLa cells. The transfection efficiency was confirmed by Western blotting (Figure 2A) and qPCR (Figure 2B). To investigate the effect of METTL3 on cell cycle progression, METTL3-knockdown and METTL3-overexpression cells were harvested 10 hours after nocodazole was added, and then, flow cytometry assays were performed. The percentage of cells in each phase of the cell cycle showed that METTL3 knockdown delayed cell cycle progression, while METTL3 overexpression significantly facilitated cell cycle progression (Figure 2C). We further carried out an H3-specific flow cytometry assay to detect whether METTL3 is necessary for the G2/M transition. As shown in Figure 2D, the knockdown of METTL3 significantly decreased the percentage of cells in the M phase, whereas overexpression of METTL3 elevated the percentage of cells in the M phase. Furthermore, colony formation and CCK-8 assays were used to detect the effect of METTL3 on cell proliferation. The results of these experiments showed that the growth
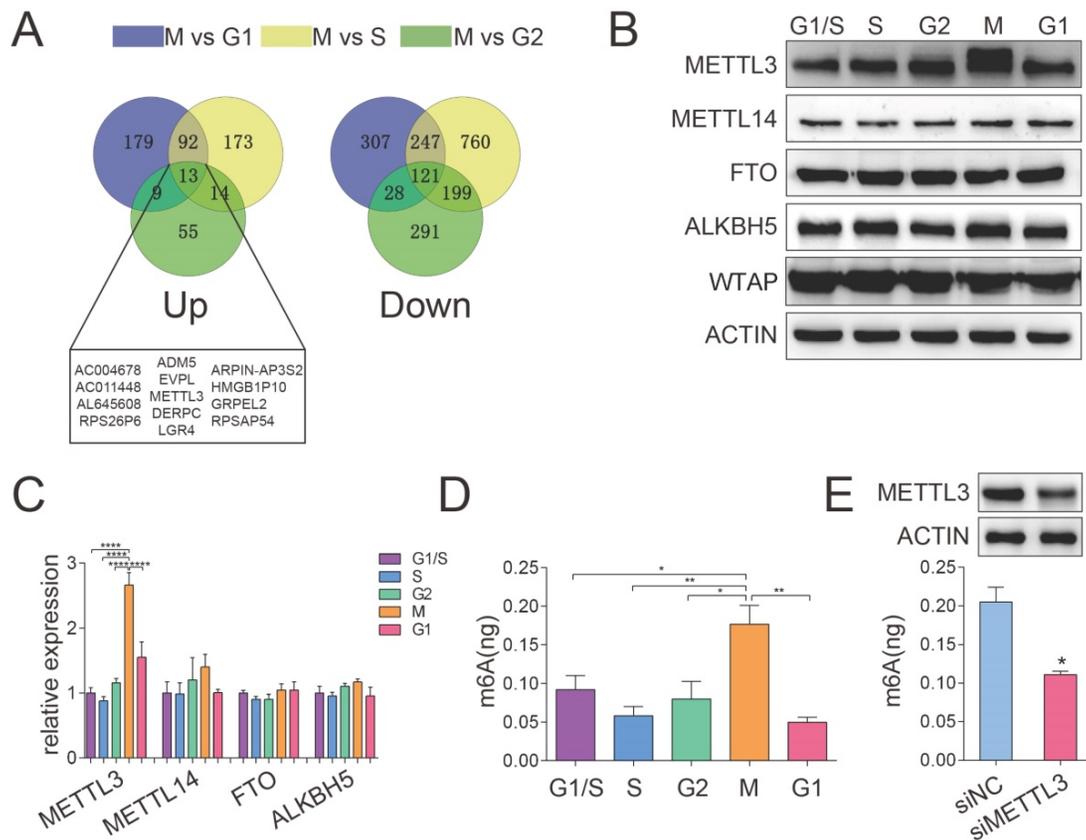

Figure 1. METTL3 expression was elevated and correlated with high m6A levels in the M phase. (A) Venn diagram illustrated the upregulated and downregulated genes differentially expressed in the M phase compared to other cell cycle phases (G1 phase, S phase and G2 phase). (B) The protein levels of METTL3, METTL14, FTO, ALKBH5 and WTAP were analyzed by Western blotting. ACTIN served as a loading control. (C) The relative mRNA levels of METTL3, METTL14, FTO and ALKBH5 were analyzed by qPCR. **** P < 0.0001 (one-way ANOVA analysis) for the indicated comparisons. Relative mRNA expression levels were normalized by 18S rRNA. Data are presented as the mean ± SD for n = 3 replicate cultures. (D) Global m6A mRNA methylation levels in various HeLa cell cycle phases were determined by m6A enzyme-linked immunosorbent assays. m6A RNA methylation quantification was performed based on the standard curve. * P < 0.05, ** P < 0.01 (one-way ANOVA analysis) for the indicated comparisons. (E) Quantification of m6A enrichment in mRNA from control and siMETTL3 cells in the M phase. The knockdown efficiency of METTL3 in HeLa cells was confirmed by Western blotting indicated in the upper panel. Quantification of m6A was detected by the m6A RNA methylation quantification kit. Data shown are mean ± SD for n = 3 replicate cultures, * P < 0.05 compared to negative control. (The western blotting data are representative of n=3 independent experiments).

and proliferation capabilities of the cells were weakened after the knockdown of METTL3 (Figure 2E and Figure 2F), while the overexpression of METTL3 exerted the opposite effect (Figure 2G and Figure 2H).

Collectively, these data suggested that METTL3 significantly facilitated cell cycle progression and promoted cell growth *in vitro*.
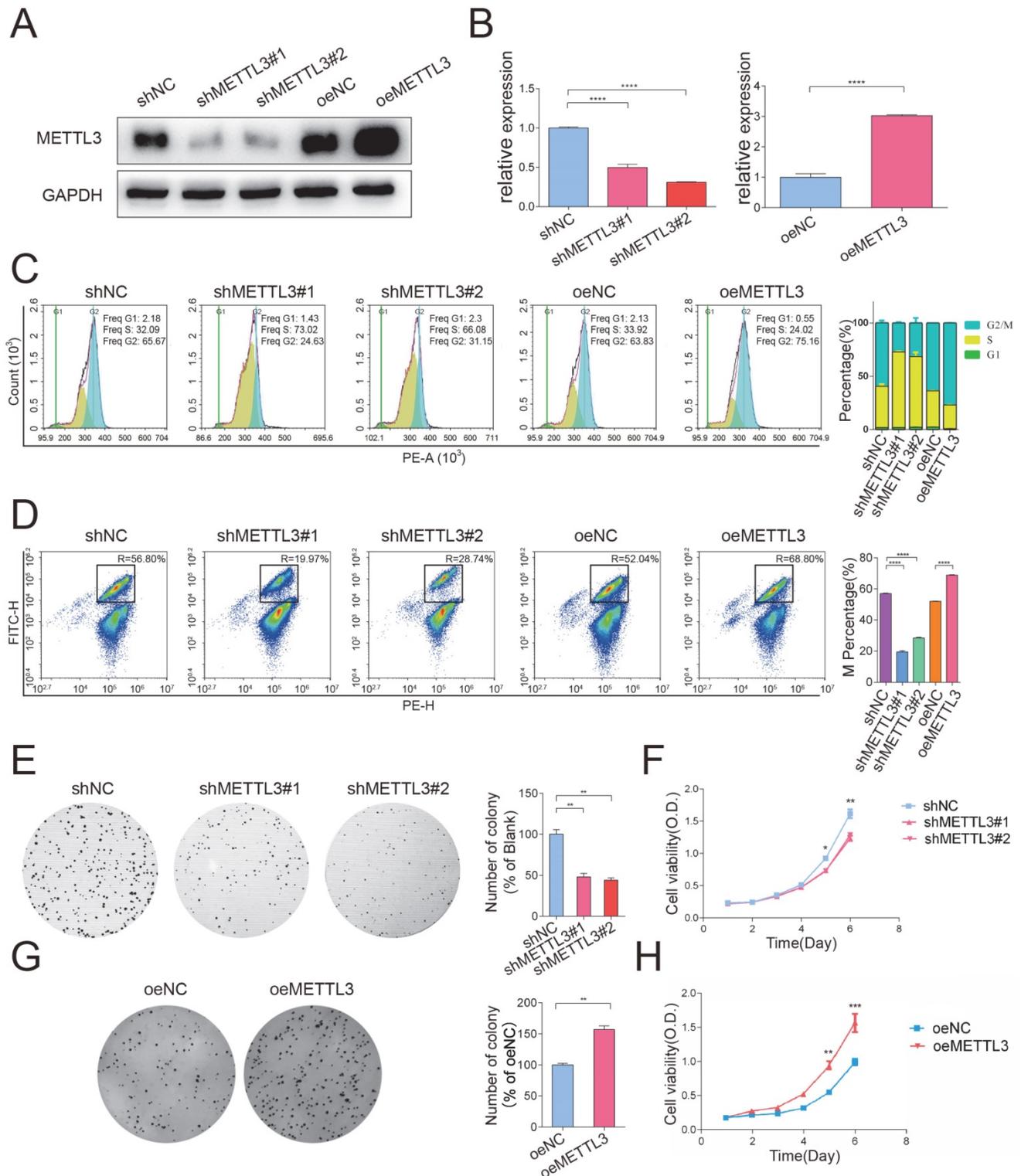

Figure 2. METTL3 facilitated cell cycle progression and promoted cell growth *in vitro*. (A) The knockdown and overexpression efficiency of METTL3 in HeLa cells was confirmed by Western blot. Western blot analysis of protein extracted from METTL3 stable knockdown and overexpression HeLa cells. The western blotting data are representative of n=3 independent experiments. (B) The knockdown and overexpression efficiency of METTL3 in HeLa cells was also confirmed by RT-qPCR analysis. Gene expression was assayed by RT-qPCR analysis of RNA extracted from METTL3 stable knockdown and overexpression HeLa cells. Data shown are mean fold-change values ± SD for n = 3 replicate cultures, with intra-sample normalization to the 18S RNA level of each sample. **** $P < 0.0001$ for the indicated comparisons. (C) Cell cycle progression after knockdown (shNC or shMETTL3) or overexpression (oeNC or oeMETTL3) of METTL3 was detected by flow cytometry. The percentage of cells in the G1, S and G2/M phases

were calculated using FACS software and data were shown in each image on the left panel. The average percentage of cells in the G1, S and G2/M phases from 3 independent experiments were shown by a stacked bar chart on the right panel. (D) The percentage of cells in the M phase was detected by phospho-H3-specific flow cytometry in METTL3-knockdown cells, METTL3-overexpression cells, and the corresponding negative control cells. The percentage of cells in the M phases showed in each image on the left panel. The average percentage of cells in the M phases from 3 independent experiments was showed by stacked bar chart on the right panel. Data shown are mean ± SD for n = 3 replicate cultures. **** P < 0.0001 (one-way ANOVA analysis) for the indicated comparisons. (E-F) Colony formation assays (E) and CCK-8 proliferation assays (F) were performed to evaluate the proliferation of HeLa cells after transfection of shMETTL3 interference plasmid. Histograms present the colony numbers of each group. Data shown on (E) the right panel are mean fold-change values ± SD for n = 3 replicate cultures. * P < 0.05 (one-way ANOVA analysis) for the indicated comparisons. (F) Data shown are mean ± SD for n = 3 replicate cultures. * P < 0.05, ** P < 0.01 for METTL3 knockdown versus control, evaluated on indicated day (one-tailed t-test). (G-H) Colony formation assays (G) and CCK-8 proliferation assays (H) were performed to evaluate the proliferation of HeLa cells after transfection of METTL3 overexpression plasmid. Histograms present the colony numbers of each group. Data shown at (G) right panel are mean fold-change values ± SD for n = 3 replicate cultures. ** P < 0.01 (unpaired Student's t-test) for the indicated comparisons. (H) Data shown are mean ± SD for n = 3 replicate cultures. ** P < 0.01, *** P < 0.001 for METTL3 overexpression versus control, evaluated on indicated day (one-tailed t-test).

Transcriptome-wide m⁶A-seq identified potential targets of METTL3

Considering that METTL3 expression was upregulated in the M phase and considering the critical role of the G2/M transition in the cell cycle [27], we used m⁶A-seq analysis of the G2 phase and M phase to investigate the potential molecular mechanism of METTL3 and to identify its downstream targets in the cell cycle. m⁶A -seq identified 34644 peaks in 15,097 genes in the G2 phase (peaks and genes identified in the G2 phase are listed in Table S3) and 33228 peaks in 14,109 genes in the M phase (peaks and genes identified in the M phase are listed in Table S4). Among these genes, 12,514 genes were common between the G2 and M phases (Figure 3A). The genomic distribution of m⁶A peaks across mRNA transcripts and the m⁶A motifs identified from the two groups (Figure 3B-3D, mapped region of each sample are shown in Figure S1D) were consistent with those reported previously [28]. Moreover, the m⁶A -seq analysis revealed that the m⁶A peaks of 1,895 transcripts were increased in the M phase compared with the G2 phase (Figure 3E and transcripts list in Table S5) (fold change > 1.5, P < 0.05) (Different m⁶A peaks and Transcription Start Sites are shown in Figure S1E, the density of Different Expression Genes is shown in Figure S1F). To obtain comprehensive gene function information, Gene Ontology (GO) analysis was conducted. The analysis revealed that the differentially m⁶A -modified genes were significantly enriched in gene sets involved in cell cycle regulation, such as "DNA damage response, signal transduction in cell cycle regulation" (P < 0.01, 0.4% of cluster frequency) and "positive regulation of mitotic cell cycle" (P < 0.01, 0.02% of cluster frequency). In addition, the m⁶A-modified genes were also involved in regulating mRNA splicing and translation, which are directly related to the functional consequence of m⁶A modification (Figure 3F and GO_BP list in Table S6).

m⁶A methylation regulated CDC25B activation

We next screened the genes listed in the cell cycle-related GO category in our data. Six genes (*SHB*, *EIF4EBP1*, *PKN2*, *PAFAH1B1*, *CDC25B*, *TERF1*) were involved in the "positive regulation of mitotic cell cycle" term. Among these genes, *CDC25B* was identified as a direct target of m⁶A modification in our in-house m⁶A -seq data and RMBase, which integrated 477,452 m⁶A modifications from 566 datasets [29]. The m⁶A peak detected near the 3'UTR of *CDC25B* was dramatically increased in the M phase compared with the G2 phase (Figure 4A). Previous studies also have shown that CDC25B plays a critical role in the G2-to-M phase transition [30], as well as cancer progression [31]. In light of such a critical role CDC25B played in cell cycle and carcinogenesis, we selected CDC25B for further investigation. To determine whether *CDC25B* is a substrate of METTL3, we validated our m⁶A -seq data by m⁶A RIP-qPCR assay. The results confirmed that the m⁶A level of *CDC25B* was markedly increased in the M phase compared with the G2 phase (Figure 4B) (P < 0.01). Moreover, the protein expression of CDC25B was upregulated in the M phase (Figure 4D). In contrast, the mRNA levels of *CDC25B* remained constant throughout the cell cycle (Figure 4C). Next, we investigated the regulation of CDC25B expression by METTL3 through Western blotting and qPCR analyses. Western blotting analysis showed that CDC25B expression was decreased when METTL3 knocked down (Figure 4E) and was significantly increased when METTL3 overexpressed (Figure 4G). However, overexpression or knockdown of METTL3 did not obviously affect the *CDC25B* mRNA levels (Figure 4F and 4H). Further, H3-specific flow cytometric analysis showed that overexpression of CDC25B was able to restore the proportion of cells in the M phase that had been significantly reduced upon knockdown of METTL3 (Figure 4I-J). Taken together, these findings proved that *CDC25B* is a downstream target of METTL3-mediated m⁶A modification and suggested that the regulation of CDC25B by METTL3 might affect translation.
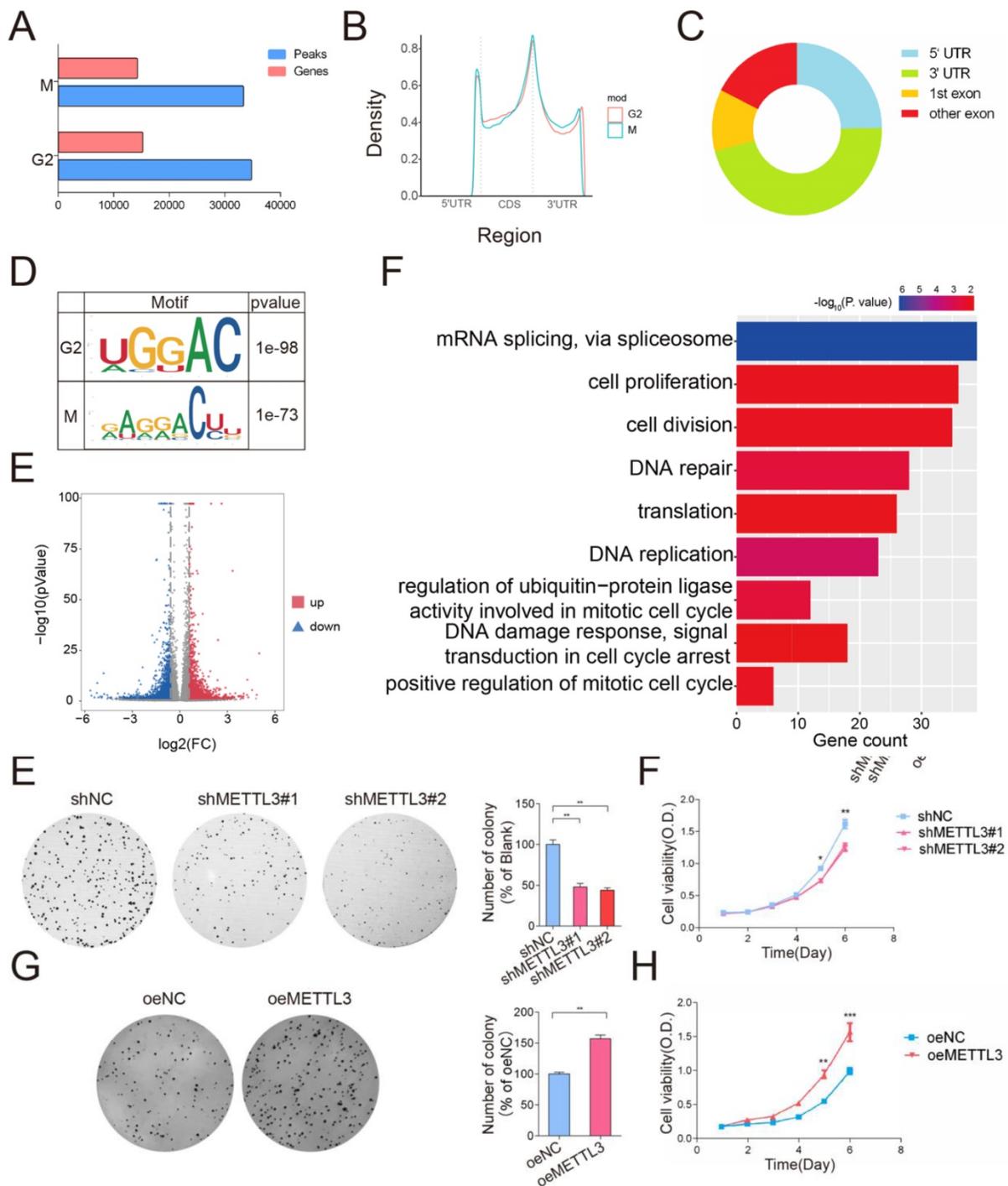
Figure 3. m⁶A -seq analysis of cells in the M and G2 phases. (A)The eluted RNA and MeRIPed RNA from HeLa cells at M or G2 phases were analyzed by deep sequencing. Bar plot showing the numbers of m⁶A peaks and m⁶A -modified genes in the M and G2 phases. (B) Density distribution of the m⁶A peak across mRNA transcripts. m⁶A peak distribution in the 5′UTR, start codon, CDS, stop codon or 3′UTR region across the entire set of mRNA transcripts**.** (C) Regions of the 5′ untranslated region (5′UTR), coding region (CDS), and 3′untranslated region (3′UTR) were split into 100 segments, then percentages of m⁶A peaks that fall within each segment were determined. Pie chart showing the different m⁶A peak distribution between the 5′UTR, exon and 3′UTR regions. (D) Predominant consensus motif GGAC was detected in both G2 phase and M phase in m⁶A-seq. (E) Volcano plot showing the distribution of genes with differential m⁶A levels in the M phase groups compared with the G2 phase group. (F) Gene ontology (GO) analysis of genes with increased m⁶A methylation levels (Fold Change > 2; P < 0.05 in m⁶A-seq) in the M phase compared to the G2 phase. Gene counts of GO terms were exhibited on the x-axis and p-values were indicated with the color of columns.

YTHDF1 enhanced *CDC25B* mRNA translation in an m⁶A-dependent manner

Previous studies have shown that the m⁶A "reader" protein YTHDF1 specifically recognizes m⁶A modification and mediates m⁶A -containing mRNA translation [19], which led us to hypothesize that the translation levels of m⁶A -modified *CDC25B* mRNA might be regulated by YTHDF1. To test our hypothesis, we conducted a loss-of-function assay by using two small interfering RNAs (siRNAs) that

targeted YTHDF1. The protein and mRNA expression levels were then examined by Western blotting and qPCR. Our analysis revealed that the protein expression of CDC25B was markedly suppressed in YTHDF1-depleted cells (Figure 5A), whereas the relative mRNA expression of *CDC25B* was not significantly different (Figure 5B). To further determine whether METTL3 enhanced *CDC25B* mRNA translation through YTHDF1, rescue experiments were carried out. We first overexpressed METTL3 in HeLa cells and then downregulated

YTHDF1 by using siRNA. The results showed that the downregulation of YTHDF1 could weaken the upregulation of CDC25B via METTL3 overexpression (Figure 5C). Functionally, consistent with the results of METTL3 knockdown, loss of YTHDF1 also delayed cell cycle progression (Figure 5D) and decreased the percentage of cells in the M phase (Figure 5E). Together, these results demonstrate that METTL3 and YTHDF1 cooperatively mediate the translational activity of *CDC25B* mRNA and further influence cell cycle progression.
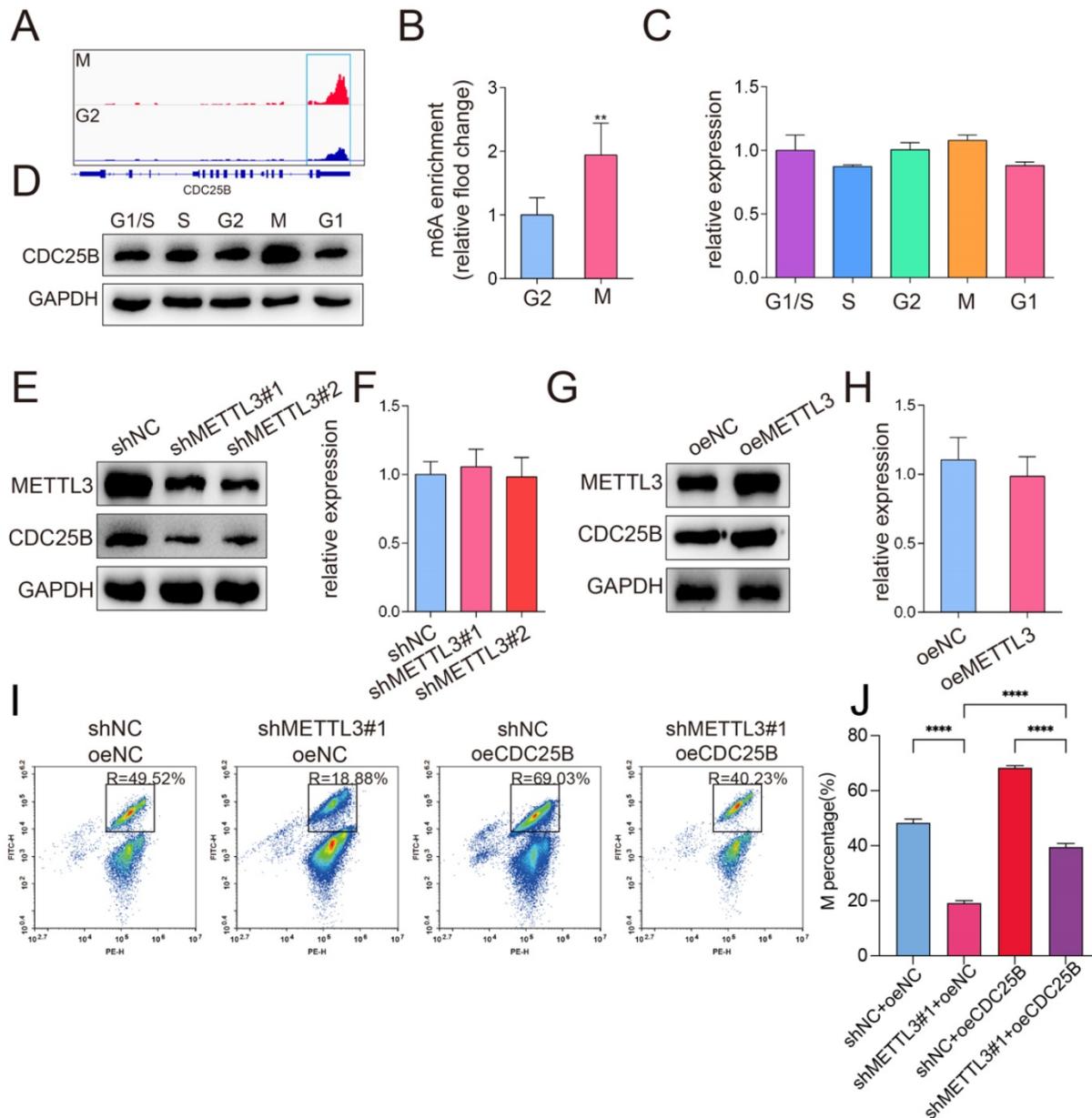

Figure 4. CDC25B was a downstream target of METTL3-mediated m⁶A modification. (A) The m⁶A abundances on *CDC25B* mRNA in the G2 phase and the M phase were plotted by IGV (Integrative Genomic Viewer). *CDC25B* mRNA had visible abundant modifications of m⁶A in the 3' UTR region in M phase cells compared to G2 phase cells. (B) The m⁶A levels of *CDC25B* in the G2 phase and the M phase were quantified by m⁶A RNA immunoprecipitation followed by RT-qPCR. The relative m⁶A level was normalized by the input. Data shown are mean fold-change values ± SD of triplicate experiments, ** P < 0.01 (unpaired Student's t-test) M verse G1 phase. (C-D) The mRNA (C) and protein (D)expression of CDC25B in various phases of the cell cycle was analyzed by RT-qPCR or Western blotting. (C) There is no significance of *CDC25B* mRNA between various phases of the cell cycle. (E) Western blotting of METTL3 and CDC25B in HeLa cells when METTL3 was knocked down. GAPDH served as a loading control. (F) qPCR analysis of *CDC25B* mRNA in HeLa cells when METTL3 was knocked down. There is no significant between the 3 groups. (G) Western blotting of METTL3 and CDC25B in HeLa cells when METTL3 was overexpressed. GAPDH served as a loading control. (H) qPCR analysis of *CDC25B* mRNA in HeLa cells when METTL3 was overexpressed. There is no significance between the two groups. (The western blotting data are representative of n=3 independent experiments). (I) The percentage of cells in the M phase was detected by
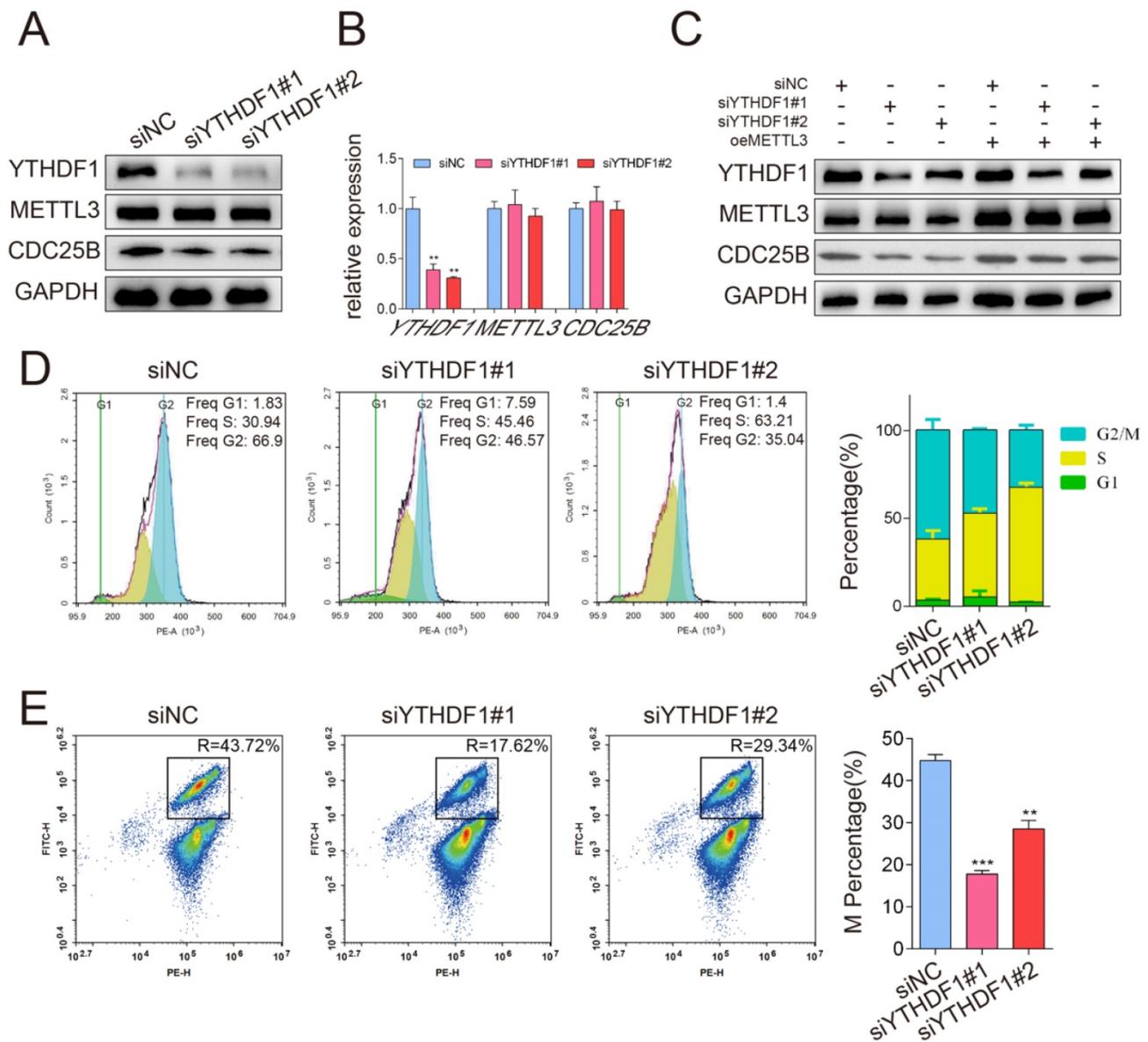
Figure 5. YTHDF1 enhanced *CDC25B* mRNA translation in an m⁶A -dependent manner. (A) Western blotting of METTL3 and CDC25B after YTHDF1 inhibition in HeLa cells. GAPDH served as a loading control. (B) RT-qPCR analysis of *METTL3* and *CDC25B* mRNA expression after YTHDF1 inhibition in HeLa cells. Data shown are mean fold-change values ± SD for n = 3 replicate cultures. ** P < 0.01 (one-way ANOVA analysis) compared to the negative control (siNC) group. (C) Analysis of the CDC25B protein expression in HeLa cells co-transfected with YTHDF1 siRNA and METTL3 plasmid. GAPDH served as a loading control. (D) Changes in the cell cycle after knockdown of YTHDF1 were detected with flow cytometry. The percentage of cells in the G1, S and G2/M phases were calculated using FACS software and data were shown in each image on the left panel. The average percentage of cells in the G1, S and G2/M phases from 3 independent experiments was shown by a stacked bar chart at the right panel. (E) The percentage of cells in the M phase after knockdown of YTHDF1 was detected by phospho-H3-specific flow cytometry. The percentage of cells in the M phases showed in each image on the left panel. The average percentage of cells in the M phases from 3 independent experiments was shown by a stacked bar chart on the right panel. Data shown are mean values ± SD for n = 3 replicate cultures. ** P < 0.01, *** P < 0.001 (one-way ANOVA analysis) compared to the negative control (siNC) group. (The western blotting data are representative of n=3 independent experiments).

METTL3 promoted tumor growth *in vivo*

To test the effect of METTL3 on tumorigenicity, we performed a subcutaneous implantation experiment in nude mice. Stable METTL3-knockdown, METTL3-overexpression and control HeLa cells were established and subcutaneously injected into the flanks of nude mice (Figure 6A).

Knockdown of METTL3 dramatically suppressed HeLa subcutaneous tumor growth in nude mice, as reflected by the significant reduction in tumor size and tumor weight, whereas METTL3 overexpression resulted in increased tumor size and tumor weight (Figure 6B-6C). In addition, consistent with the results of the *in vitro* experiment, the expression of CDC25B was decreased in METTL3-knockdown tumors but

significantly increased in METTL3-overexpression tumors (Figure 6D). The results from the knockdown and overexpression models led us to conclude that

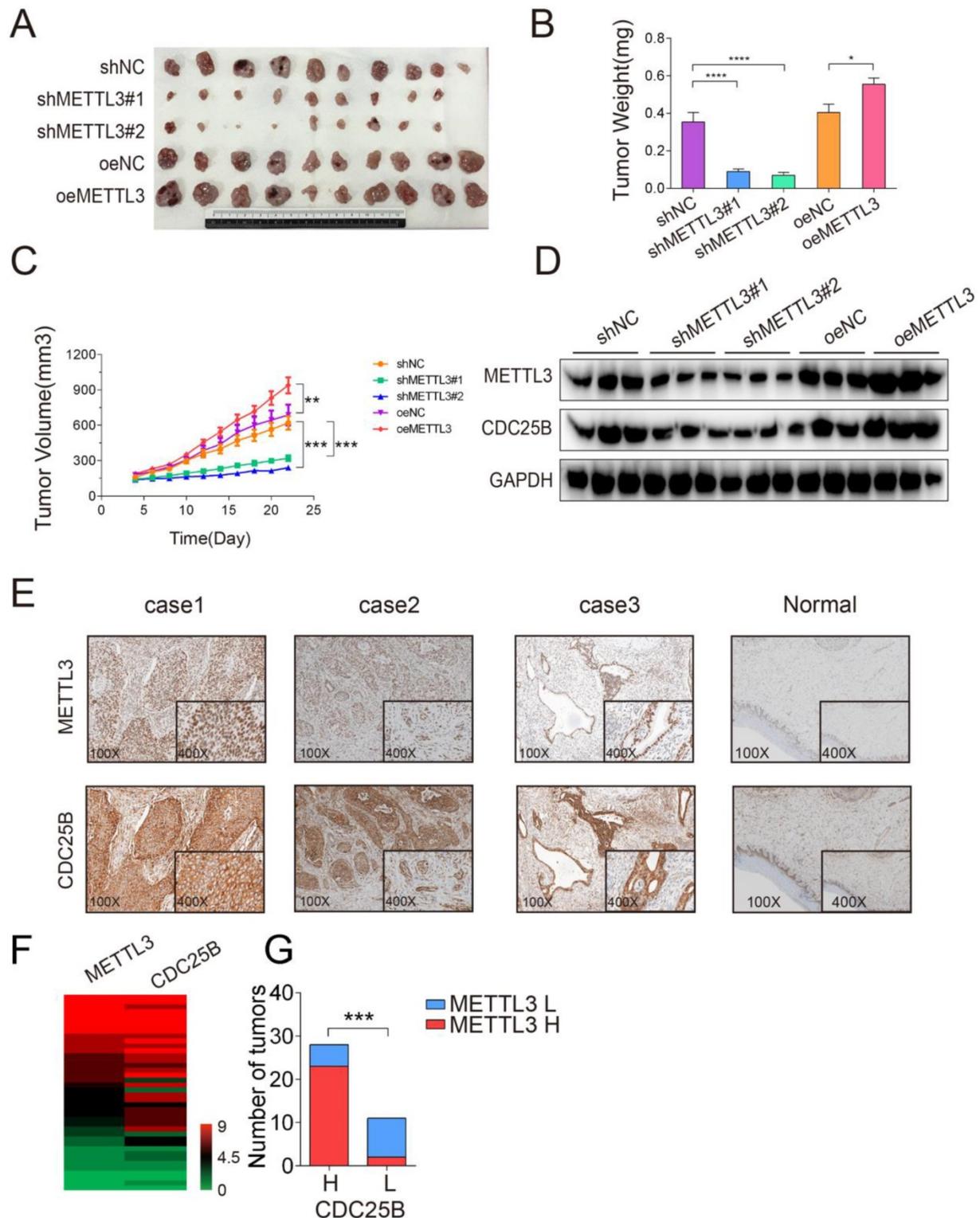METTL3 played a critical role in promoting tumor growth *in vivo*.

Figure 6. METTL3 promoted tumor growth *in vivo*. (A) Representative images of subcutaneous HeLa tumors growth in xenografted BALB/c nude mice. Each group of mice was ectopically implanted with 5 × 10⁶ indicated cells into the flanks of mice (n > 9). Here, cells were transfected with shRNA (shNC or shMETTL3) or overexpression (oeNC or oeMETTL3) lentiviral vector. (B) Tumors were harvested 22 days after cell injection, and the weights of the tumors that formed in the subcutaneously implanted mouse model were measured. The data are presented as the mean ± SEM tumor weight, * P < 0.05, **** P < 0.0001(one-way ANOVA analysis) for the indicated comparisons. (C) The size of the tumors that formed in the subcutaneously implanted mouse model was monitored every 2 days. The data are presented as the mean ± SEM tumor volume, ** P < 0.01, *** P < 0.001(one-tailed t-test) for the indicated comparisons. (D) Western blotting assay of METTL3 and CDC25B protein expression in the tumors from each group. Data are representative of 3 different tumors from each group. GAPDH served as a loading control. (E) Immunohistochemical staining of the METTL3 and CDC25B protein in human

Based on the mechanism we identified above, we proceeded to explore the clinical relevance of METTL3 and CDC25B in patient samples. Immunohistochemistry (IHC) staining of 39 clinical human cervical tumor tissues revealed that both METTL3 and CDC25B are moderately or highly expressed in most of the cervical cancer samples, whereas their expression is weak or not detectable in the superficial or intermediate squamous epithelial cell layer of the cervix (Fig. 6E). Interestingly, METTL3 and CDC25B are also moderately expressed in the normal parabasal/basal cell layer of the cervix squamous epithelium. The parabasal/basal cell layer is potentially generative mitotic activity may be seen (MIB-1 positivity) [32]. This implies that METL3 and CDC25B are expressed in cells with high mitotic activity, whether it is tumor cells or normal cells. We further investigated the association between METTL3-CDC25B expression in cervical cancer samples. The immunohistochemical staining of METTL3 and CDC25B was categorized into either high or low expression, according to the IHC score, and the IHC scores of 39 samples are summarized in a heatmap (Figure 6F) (the final score was defined as the staining number score multiplied by the staining color score). Interestingly, high METTL3 expression tumors had high CDC25B (Figure 6G, P < 0.001) expression levels. Taken together, METTL3 and CDC25B expression are upregulated in human cervical cancer samples and the expression of CDC25B was related to that of METTL3.

Discussion

Dysregulation of the cell cycle underlies the aberrant cell proliferation that characterizes cancer cells. Analysis of DNA replication-related molecules in cancer is now leading to the identification of novel biomarkers for cancer detection and is providing validated targets for cell cycle-targeted therapies. Here, we investigated the dynamic changes of gene mRNA levels in the cell cycle by RNA-seq analysis. We found that the mRNA and protein levels of METTL3 were significantly increased, which was associated with the highest m^{6}A level in the M phase. Furthermore, METTL3 activation of the M-phase inducer CDC25B was dependent on YTHDF1-mediated m^{6}A methylation, as determined by m^{6}A sequencing and m^{6}A MeRIP-qPCR assays. The expression of METTL3 is correlated with the expression of CDC25B in cervix cancer.

Recent studies have shown that depletion of YTHDF2 leads to the delay of mitotic entry due to the overaccumulation of negative regulators of the cell cycle, such as WEE1 [33]. Another study established that the demethylase FTO can phosphorylate and regulate *CCND1* and finally affect the G1 phase process [22]. Le et al. proved that WTAP was involved in cell cycle arrest induced by TGFβ exposure, and SMAD2/3, JunB might be the targets of WTAP [34]. Due to the short duration of cell division and the limitation of the synchronization method of previous studies, it remains unclear whether m^{6}A is involved in the regulation of each cell cycle division. In the present study, we generated a cell cycle synchronization model using a thymine double blockade combined with a mitotic inhibitor to accurately capture the phases of cell cycle division. Stable expression of METTL3 in the G1, S and G2 phases was observed, which was consistent with previously reported experimental data and supported the reliability of this study [33]. In the M phase samples collected with mitotic inhibitor specificity, we found an interesting phenomenon in which high expression of the methyltransferase METTL3 mediated an increase in methylation levels. Previous studies have shown that METTL3 promotes the proliferation of many types of cancer cells, such as liver, colon and gastric cancers [26, 35, 36]. However, the regulation of METTL3 in the M phase has not been reported. In this study, we confirmed the regulatory effect of METTL3 on the M phase by using flow cytometry with a phosphorylated histone H3 antibody.

To explore the specific molecular mechanism by which METTL3 regulates the cell cycle, we performed methylation sequencing on samples in the G2 and M phases. The results showed that differentially methylated genes in the G2 and M phases are highly enriched in the cell cycle, cell proliferation and other related functions. In previous studies, the differentially expressed genes after METTL3 knockdown were significantly enriched in cell cycle-related functions, which also suggested the important role of METTL3 in the cell cycle [37]. After further analysis of genes with differentially increased methylation levels in the M phase, we found that *CDC25B* is a candidate molecule for METTL3-mediated m^{6}A modification during the M phase, and the methylation levels of its 3'UTR are increased during the M phase. As a key molecule involved in the regulation of the G2/M phase, CDC25B mainly affects G2-to-M phase switching by regulating the CDK1/CyclinB1 complex [5]. Studies have shown that the mRNA level of *CDC25B* is constant during the

cell cycle, while the protein level increases in the M phase, which is consistent with the results we observed [8]. Follow-up experiments confirmed the regulatory effect of METTL3 on the protein expression level of CDC25B. It is known that the methylation recognition protein YTHDF1 can selectively recognize the methylation modification at the 3'UTR of the mRNA to regulate the translation level of the modified mRNA [38]. This suggests that YTHDF1 is involved in the regulation of *CDC25B* via METTL3-mediated m6A modification. After YTHDF1 knockdown, the CDC25B protein level was downregulated concurrently with a decrease in the proportion of cells in the M phase. The above findings reveal new mechanisms by which METTL3-mediated m6A modification regulates the cell cycle.

Our *in vitro* and *in vivo* data revealed that regulation of the METTL3-m6A-CDC25B axis resulted in the adjustment to the proliferation of cancer cells. In light of the fact that the regulation of CDC25B expression by METTL3 in this study occurs at the translational level, we found METTL3 has no effect on the mRNA level of CDC25B. Therefore, previously RNAseq databases analysis could not find the role of METTL3 in regulating CDC25B. Furthermore, using an immunochemistry assay, we showed that the protein expression of METTL3 was related to CDC25B expression in cervical cancer specimens. These findings confirm that the METTL3-m6A-CDC25B axis is essential for the growth and maintenance of cancer cells and tumor progression.

In summary, this study demonstrates the role of METTL3 in phase transition during the cell cycle and reveals a novel METTL3/m6A/CDC25B pathway that is involved in cell cycle regulation. Our results not only broaden the understanding of m6A modification biology but also provide new targets for tumor diagnosis and treatment.

Materials and Methods

Human cervical tumor samples and cell culture

Samples were collected from patients who underwent surgery at the Shanghai First Maternity and Infant Hospital from 2014 to 2019, and the study was approved by the Institutional Ethics Committee of Shanghai First Maternity and Infant Hospital. The study was compliant with all the relevant ethical regulations regarding research involving human participants. Human cervical cancer HeLa cells and HEK-293T cells (#CCL-13&#FS-0156, ATCC, Rockville, MD, USA) were cultured in Dulbecco's modified Eagle's medium (DMEM) containing 10% fetal bovine serum (FBS) and 1% penicillin/ streptomycin (#10378016, Gibco, Grand Island, NY, USA). All the cells were maintained in an atmosphere containing 5% CO_2 at 37°C.

Cell cycle synchronization

The cells were synchronized by the double-block method with thymidine and nocodazole as described in our previous study [25]. Briefly, for the first block, HeLa cells were plated at 60% confluence and incubated in the presence of 2.5 mM thymidine for 18 hours. The cells were washed with PBS three times and released in the thymidine-free medium for 10 hours. For the second block, the cells were treated with 2.5 mM thymidine for 16 hours. The cells were considered synchronized at the G1/S boundary. Cells in the S phase and G1 phase were collected 4 and 15 hours later, respectively. Cells in the G2 phase were collected after being released and treated with nocodazole (100 ng/ml) for 8 h, and cells in the M phase were collected after being released and treated with nocodazole for 10 hours.

Plasmids, siRNAs and transfection

Expression and purification of lentiviruses were performed as described in the manufacturer's protocol. For the generation of lentivirus encoding short hairpin RNA (shRNA) targeting METTL3, corresponding shRNA oligos were cloned into the pLKO.l vector (#8453, Addgene, Watertown, MA, USA). For lentiviral vectors expressing METTL3 and luciferase (control), the corresponding cDNA was cloned into the pKD-Puro-FLAG vector. To generate METTL3 stable knockdown and overexpression cells, HeLa cells were infected with lentivirus and selected with puromycin. Specific siRNAs targeting YTHDF1, and the control siRNA were purchased from IGE BIO (Guangzhou, China). Cell transfection was achieved by using Lipofectamine 2000 (#11668019, Invitrogen, Carlsbad, CA, USA) according to the manufacturer's protocol. All the shRNA and siRNA sequences are listed in Table S1.

RT-Quantitative PCR

RT-qPCR was performed as described in our previous study [39]. RNA was extracted according to the TRIzol RNA isolation protocol, cDNA was synthesized with a reverse transcriptase kit, and real-time PCR was performed with an SYBR Premix Ex Taq Kit (#RR820, Takara, Tokyo, Japan) in a CFX96 Real-Time PCR System (#185-5195, Bio-Rad, Hercules, CA, USA). Target gene expression levels were normalized against that of the 18S rRNA gene, and relative expression was calculated using the 2-ddCt method. All the primer sequences are listed in Table S2.

Western blotting

Western blotting was performed as described in our previous study [40]. Briefly, total protein lysates were prepared from cells with SDS buffer with proteinase. A BCA assay (P1002, Beyotime, Shanghai, China) was performed to quantify the protein concentrations. The obtained protein samples were resolved using 10% SDS-PAGE and transferred onto a PVDF membrane (#ISEQ00010, Millipore, Temecula, CA, USA). After being blocked with 5% fat-free milk, the membranes were cut into strips with molecular weight cut in half in-between the strips. Then, the strips were incubated overnight at 4°C with primary antibodies (the antibodies information was listed in Table S7). After incubation with secondary antibodies, the immunoreactive bands were visualized using an enhanced chemiluminescence reagent (WBKIS0100, Millipore, Temecula, CA, USA). The densities of the immunoreactive bands were determined by Quantity One 1-D Analysis Software, (RRID:SCR_014280).

Measurement of the m6A levels

The m6A levels in the total RNA were detected using a commercial m6A RNA methylation quantification kit (#P9005, Epigentek, NY, USA). Briefly, 250 ng of total RNA was added to each well, and capture antibody solution and detection antibody solution were added according to the manufacturer's protocol. The absorbance of each well at a wavelength of 450 nm was measured to determine the m6A level, and then calculations were performed based on the standard curve.

Flow cytometric cell cycle analysis

Briefly, cells were fixed in 70% alcohol overnight at -20°C and then incubated with 50 μg/ml propidium iodide (PI) and 100 μg/ml RNase A in the dark for 10 minutes. Cell cycle phase distribution was assessed using a FACScan flow cytometer (#342973, BD Biosciences, Franklin Lakes, NJ, USA). For the flow cytometry analysis of the M phase, fixed cells were treated with 0.25% Triton X-100 on ice for 15 minutes and then incubated with phospho-H3 antibody (#3465, CST, Danvers, MA, USA) (1:1500 in 1% BSA) for 3 hours at room temperature. The H3P-labeled cells were subsequently stained with PI and analyzed on a flow cytometer.

CCK-8 assay

Cell proliferation was detected using a Cell Counting Kit-8 (CCK-8) assay according to the manufacturer's instructions. Briefly, cells were seeded into a 96-well plate at a density of 5000 cells/well. Cell growth was tested every day by adding 10 μl/well CCK-8 (#C0039, Beyotime, Shanghai, China), and the absorbance was read at 450 nm with a microplate reader (#ELX800, BioTek, Winooski, VT, USA). The average value was calculated from 5 replicates, and a growth curve was generated from the average values.

Colony formation assay

A total of 400 cells were seeded in one well of a 6-well plate and maintained in the medium containing 10% FBS. After 2 weeks, the cells were fixed with 4% formaldehyde and stained with 0.1% crystal violet (#C0121, Beyotime, Shanghai, China). The number of colonies (defined as containing more than 50 cells) was determined under a light microscope, and each group included triplicate wells.

RNA-sequencing (RNA-seq) and m6A sequencing (m6A-seq)

Based on the documented procedure, total RNA was extracted using TRIzol reagent (#15596026, Invitrogen, Carlsbad, CA, USA). The RNA-seq was performed using two biological replicate pools for each cell cycle phase, with each pool representing RNA from individual samples (n=3). The quality and quantity of the total RNA were detected using an RNA 6000 Nano LabChip Kit (#5067, Agilent, Santa Clara, CA, USA). A cDNA library was constructed and then sequenced with a Hiseq 4000 system (Illumina, CA, USA). Differentially expressed genes (DEGs) were identified using the DESeq2 package in R with thresholds pf a Benjamini-Hochberg adjusted p value <0.05 and a two fold change in expression. For m6A-seq, mRNA was purified using the Dynabeads mRNA Purification Kit (#61006, Thermo Fisher, Waltham, MA, USA). An anti-m6A antibody was used for the immunoprecipitation of m6A -modified mRNA. The input and immunoprecipitation samples were both used to construct the libraries. Then, the eluted RNA and MeRIPed RNA were analyzed by deep sequencing on an Illumina NovaseqTM 6000 platform at LC-BIO Ltd. (Hangzhou, China) following the vendor's recommended protocol. Reads were mapped to the human reference genome (GRC38) using R language, version 3.8.1. We filtered the differentially expressed peak genes based on a false discovery rate (FDR) of <0.05.

MeRIP-qPCR

m6A modification of individual genes was assessed using a MeRIP-qPCR assay. Briefly, mRNA was purified from total RNA, and one-tenth of the RNA was saved as input control. After the RNA was fragmented, it was immunoprecipitated with an anti-m6A antibody or IgG coupled to Dynabeads (#1001, Thermo Fisher, Waltham, MA, USA). Further enrichment was calculated by qPCR, and the relative m6A enrichment in each sample was calculated by

normalizing to the input.

Tumorigenicity in nude mice

BALB/c-nu female mice (6 weeks old) (Hua Fu Kang, Beijing, China) were maintained in a specific pathogen-free animal room at the Jinan University Animal Center. Animal care and experimental procedures were approved by the Institutional Animal Care and Use Committees. Briefly, for the subcutaneously injected model, 5×10^6 cells were injected into the flanks of the mice. The body weight and tumor volume were measured every two days. Tumor volume was assessed as $(L \times W^2/2)$, where L and W represent the length and width, respectively. All the animals were killed at the end of the study, and their tumors were collected for further analysis.

Histological and immunohistochemical (IHC) staining

Cervical cancer samples were cut into 4-µm-thick sections and placed on pathological slides for immunohistochemical staining. The sections were heated at 100°C in citrate buffer solution (pH=6.0) for 10 minutes to facilitate antigen retrieval. Then, the sections were incubated with rabbit antibodies against human METTL3 (EPR18810, Abcam, Cambridge, UK) and CDC25B (EPR3459(2), Abcam, Cambridge, UK) for 3 h followed by incubation with secondary antibodies (Dako REAL EnVision, USA). The immunoreacted cells were visualized using diaminobenzidine, and the nuclei were counterstained with hematoxylin. Phosphate-buffered saline (PBS) was substituted for the primary antibody as a negative control.

IHC scores

To show the extent of immunostaining with indicated proteins anti-body, a semi-quantitative score was established. For this purpose, each sample was scored: (a) for the percentage of labeled cancer cells (0=absence; 1=less than 30%; 2=30–60%; and 3=more than 60%); and (b) and for the intensity of the immunostaining (0=no staining; 1=weak; 2=mild; and 3=strong staining). Multiplication of both scores allowed the final scoring of samples, ranging from 0 to 9. The expressions of indicated proteins were categorized as "low" for the score of "below 4.5" versus "high" for score of "above 4.5". Analysis was performed by two independent pathologists.

Statistical analysis

The data were graphed using GraphPad Prism 6 (RRID:SCR_002798) and analyzed to determine statistical significance by one-way analysis of variance (ANOVA) (for 3 or more comparisons) or one-tailed Student's t-test (for 2 group comparisons). The Kaplan-Meier method and log-rank tests were used to compare overall survival. $p<0.05$ was considered statistically significant. All the experiments were performed at least in triplicate. The data and error bars are presented as the mean ± standard deviation (SD) or standard error of the mean (S.E.M).

Supplementary Material

Supplementary figure and tables.
https://www.ijbs.com/v18p3223s1.pdf

Author Contributions

BD and ZDX conceived of the study and designed the experiments jointly. HFL, YZ, GXC, HZS, YYL, LFL, PDY and JLC carried out the experimental work. HFL, GXC, and BD did data analysis. HFL, YZ and GXC prepared the figures for publication. HFL, GXC, ZDX and BD drafted the manuscript jointly. BD supervised the overall project and edited the final manuscript.

Data Availability

The m^{6}A-seq data have been deposited in the Sequence Read Archive (SRA) repository under the submission numbers: PRJNA754703.

Competing Interests

The authors have declared that no competing interest exists.

References

1. Hanahan D, Weinberg RA. Hallmarks of cancer: the next generation. Cell. 2011; 144: 646-74.
2. Smith JA. The cell cycle and related concepts in cell proliferation. J Pathol. 1982 136: 149-66.
3. Israels ED, Israels LG. The cell cycle. Stem cells (Dayton, Ohio). 2001; 19: 88-91.
4. Grana X, Reddy EP. Cell cycle control in mammalian cells: role of cyclins, cyclin dependent kinases (CDKs), growth suppressor genes and cyclin-dependent kinase inhibitors (CKIs). Oncogene. 1995; 11: 211-9.
5. Galaktionov K, Beach D. Specific activation of cdc25 tyrosine phosphatases by B-type cyclins: evidence for multiple roles of mitotic cyclins. Cell. 1991; 67: 1181-94.
6. Aressy B, Ducommun B. Cell cycle control by the CDC25 phosphatases. Anticancer Agents Med Chem. 2008; 8: 818-24.
7. Wang M, Zhu XY, Wang L, Lin Y. Expression and significance of CDC25B, PED/PEA-15 in esophageal carcinoma. Cancer Biother Radiopharm. 2015; 30: 139-45.
8. Gasparotto D, Maestro R Fau - Piccinin S, Piccinin S Fau - Vukosavljevic T, Vukosavljevic T Fau - Barzan L, Barzan L Fau - Sulfaro S, Sulfaro S Fau - Boiocchi M, et al. Overexpression of CDC25A and CDC25B in head and neck cancers. Cancer Res. 1997; 15: 2366-8.
9. Takemasa I, Yamamoto H, Sekimoto M, Ohue M, Noura S, Miyake Y, et al. Overexpression of CDC25B phosphatase as a novel marker of poor prognosis of human colorectal carcinoma. Cancer Res. 2000; 60: 3043-50.
10. Boutros R, Lobjois V, Ducommun B. CDC25 phosphatases in cancer cells: key players? Good targets? Nat Rev Cancer. 2007; 7: 495-507.
11. Roskoski R, Jr. Cyclin-dependent protein kinase inhibitors including palbociclib as anticancer drugs. Pharmacol Res. 2016; 107: 249-75.

12.　Schwartz GK, Shah MA. Targeting the cell cycle: a new approach to cancer therapy. Journal of clinical oncology : official journal of the American Society of Clinical Oncology. 2005 23: 9408-21.

13.　Maity A, Das B. N6-methyladenosine modification in mRNA: machinery, function and implications for health and diseases. The FEBS journal. 2016; 283: 1607-30.

14.　Yang Y, Hsu PJ, Chen YS, Yang YG. Dynamic transcriptomic m(6)A decoration: writers, erasers, readers and functions in RNA metabolism. Cell Res. 2018; 28: 616-24.

15.　Stoilov P, Rafalska I, Stamm S. YTH: a new domain in nuclear proteins. Trends Biochem Sci. 2002; 27: 495-7.

16.　Wang X, Feng J, Xue Y, Guan Z, Zhang D, Liu Z, et al. Structural basis of N(6)-adenosine methylation by the METTL3-METTL14 complex. Nature. 2016; 534: 575-8.

17.　Zheng G, Dahl JA, Niu Y, Fedorcsak P, Huang CM, Li CJ, et al. ALKBH5 is a mammalian RNA demethylase that impacts RNA metabolism and mouse fertility. Mol Cell. 2013; 49: 18-29.

18.　Chen J, Du B. Novel positioning from obesity to cancer: FTO, an m(6)A RNA demethylase, regulates tumour progression. J Cancer Res Clin Oncol. 2019; 145: 19-29.

19.　Shi H, Wei J, He C. Where, When, and How: Context-Dependent Functions of RNA Methylation Writers, Readers, and Erasers. Mol Cell. 2019; 74: 640-50.

20.　Yang J, Chen J, Fei X, Wang X, Wang K. N6-methyladenine RNA modification and cancer. Oncol Lett. 2020; 20: 1504-12.

21.　Cao G, Li HB, Yin Z, Flavell RA. Recent advances in dynamic m6A RNA modification. Open Biol. 2016; 6: 160003.

22.　Hirayama M, Wei FY, Chujo T, Oki S, Yakita M, Kobayashi D, et al. FTO Demethylates Cyclin D1 mRNA and Controls Cell-Cycle Progression. Cell Rep. 2020; 31: 107464.

23.　Shi Y, Fan S, Wu M, Zuo Z, Li X, Jiang L, et al. YTHDF1 links hypoxia adaptation and non-small cell lung cancer progression. Nature communications. 2019; 10: 4892.

24.　Yang Z, Wang T, Wu D, Min Z, Tan J, Yu B. RNA N6-methyladenosine reader IGF2BP3 regulates cell cycle and angiogenesis in colon cancer. J Exp Clin Cancer Res. 2020; 39: 203.

25.　Zhong Y, Yang J, Xu WW, Wang Y, Zheng CC, Li B, et al. KCTD12 promotes tumorigenesis by facilitating CDC25B/CDK1/Aurora A-dependent G2/M transition. Oncogene. 2017; 36: 6177-89.

26.　Chen M, Wei L, Law CT, Tsang FH, Shen J, Cheng CL, et al. RNA N6-methyladenosine methyltransferase-like 3 promotes liver cancer progression through YTHDF2-dependent posttranscriptional silencing of SOCS2. Hepatology. 2018; 67: 2254-70.

27.　William R Taylor GRS. Regulation of the G2/M transition by p53. Oncogene. 2001; 20: 1803 ± 15.

28.　Su R, Dong L, Li C, Nachtergaele S, Wunderlich M, Qing Y, et al. R-2HG Exhibits Anti-tumor Activity by Targeting FTO/m(6)A/MYC/CEBPA Signaling. Cell. 2018; 172: 90-105.e23.

29.　Xuan JJ, Sun WJ, Lin PH, Zhou KR, Liu S, Zheng LL, et al. RMBase v2.0: deciphering the map of RNA modifications from epitranscriptome sequencing data. Nucleic Acids Res. 2018; 46: D327-D34.

30.　Mailand N, Podtelejnikov AV, Groth A, Mann M, Bartek J, Lukas J. Regulation of G(2)/M events by Cdc25A through phosphorylation-dependent modulation of its stability. EMBO J. 2002; 21: 5911-20.

31.　Chen RQ, Yang QK, Lu BW, Yi W, Cantin G, Chen YL, et al. CDC25B mediates rapamycin-induced oncogenic responses in cancer cells. Cancer Res. 2009; 69: 2663-8.

32.　Mittal K. Utility of proliferation-associated marker MIB-1 in evaluating lesions of the uterine cervix. Adv Anat Pathol. 1999; 6: 177-85.

33.　Fei Q, Zou Z, Roundtree IA, Sun HL, He C. YTHDF2 promotes mitotic entry and is regulated by cell cycle mediators. PLoS Biol. 2020; 18: e3000664.

34.　Li L, Chen YX, Yang B, Liao JY, Peng JW, Zhu S. The crosstalk between RNA m(6)A epitranscriptome and TGFbeta signaling pathway contributes to the arrest of cell cycle. Gene. 2020; 738: 144483.

35.　Li T, Hu PS, Zuo Z, Lin JF, Li X, Wu QN, et al. METTL3 facilitates tumor progression via an m(6)A-IGF2BP2-dependent mechanism in colorectal carcinoma. Mol Cancer. 2019; 18: 112.

36.　Yue B, Song C, Yang L, Cui R, Cheng X, Zhang Z, et al. METTL3-mediated N6-methyladenosine modification is critical for epithelial-mesenchymal transition and metastasis of gastric cancer. Mol Cancer. 2019; 18: 142.

37.　Lin X, Chai G, Wu Y, Li J, Chen F, Liu J, et al. RNA m(6)A methylation regulates the epithelial mesenchymal transition of cancer cells and translation of Snail. Nat Commun. 2019; 10: 2065.

38.　Adamson ED, Mercola D. Egr1 transcription factor: multiple roles in prostate tumor cell growth and survival. Tumour Biol. 2002; 23: 93-102.

39.　Yin P, Li H, Ke C, Cao G, Xin X, Hu J, et al. Intranasal Delivery of Immunotherapeutic Nanoformulations for Treatment of Glioma Through *in situ* Activation of Immune Response. Int J Nanomedicine. 2020; 15: 1499-515.

40.　Cao G, Li S, Shi H, Yin P, Chen J, Li H, et al. Schisandrin B attenuates renal fibrosis via miR-30e-mediated inhibition of EMT. Toxicol Appl Pharmacol. 2019; 385: 114769.